# Reentrant superspin glass state and magnetization steps in the oxyborate $Co_2AlBO_5$

Jitender Kumar,[1] Soumendra Nath Panja,[1] Deepak John Mukkattukavil,[1] Arpan Bhattacharyya,[2] A. K. Nigam,[3] and Sunil Nair[1,4,*]

[1]*Department of Physics, Indian Institute of Science Education and Research, Dr. Homi Bhabha Road, Pune 411008, India*

[2]*Saha Institute of Nuclear Physics, 1/AF Bidhannagar, Kolkata, India*

[3]*Department of Condensed Matter Physics and Materials Science, Tata Institute of Fundamental Research, Dr. Homi Bhabha Road, Mumbai 400 005, India*

[4]*Centre for Energy Science, Indian Institute of Science Education and Research, Dr. Homi Bhabha Road, Pune 411008, India*

(Received 16 December 2016; published 10 April 2017; corrected 28 February 2019)

An oxyborate $Co_2AlBO_5$ belonging to the ludwigite family is investigated using structural, thermodynamic, dielectric, and magnetic measurements. Magnetic measurements indicate that this system is seen to exhibit long-range magnetic ordering at $T_N = 42$ K, signatures of which are also seen in the specific heat, dielectric susceptibility, and lattice parameters. The absence of a structural phase transition down to the lowest measured temperatures distinguishes it from the more extensively investigated Fe-based ludwigites. At low temperatures, the system is seen to stabilize in a reentrant superspin glass phase at $T_G = 10.6$ K from within the magnetically ordered state. This ground state is also characterized by magnetic-field-induced metamagnetic transitions, which at the lowest measured temperatures exhibit a number of sharp magnetization steps, reminiscent of that observed in the mixed valent manganites.

DOI: 10.1103/PhysRevB.95.144409

## I. INTRODUCTION

The anisotropy inherent to different structural motifs plays a critical role in determining the electronic and magnetic ground states of a number of strongly correlated electron systems. The complex interplay between the spin, charge, and lattice degrees of freedom in such restricted geometries is known to give rise to phenomena ranging from unconventional superconductivity to novel spin and charge density waves. Oxyborates of the form $M_2M'BO_5$ crystallizing in the ludwigite structure constitute one such family of strongly correlated oxides, which have attracted interest in the recent years [1–4]. Here, $M$ and $M'$ are divalent and trivalent metals, respectively, which drive the electronic and magnetic properties of these systems. Systems in which $M$ and $M'$ are made up of the same element are called homometallic ludwigites, with $Co_3BO_5$ and $Fe_3BO_5$ being the most investigated examples. Though both of them crystallize in the same orthorhombic symmetry, the magnetic and structural properties vary considerably [4–6]. For instance, on cooling from room temperature, $Fe_3BO_5$ first exhibits a structural transition (at ≈280 K), followed by a couple of low-temperature magnetic transitions (at 112 K and 70 K) associated with the progressive ordering of Fe on different crystallographic sites. On the other hand, $Co_3BO_5$ is reported to exhibit a single magnetic transition at ≈45 K. Though the interactions are predominantly antiferromagnetic, static and dynamic susceptibility measurements on both of these systems indicate that a weak ferromagnetic component exists along with long-range antiferromagnetic order. The heterometallic ludwigites, where $M$ and $M'$ are made up of different elements, can be broadly divided into two types. In some systems, both $M$ and $M'$ are magnetic (for instance, $M$ = Co, Ni, Mn, or Cu, and $M'$ = Fe, Ni, or Cr) and both these species appear to participate in the observed magnetic order [7–9]. The other type comprises systems in which $M'$ is nonmagnetic (for instance, Ga, Al, Mg, or Ti), and the resultant dilution of the magnetic lattice typically manifests itself in the form of a reduced transition temperature [10–13]. Since the $M$ ions have four inequivalent crystallographic sites within the ludwigite structure, the eventual properties are likely to be crucially influenced by the occupancies of the different $M$ and $M'$ species within these sites. In some ludwigites, this is also reported to give rise to a low-temperature spin-glass-like state without long-range order [11,13].

A defining feature of the ludwigite structure is the presence of a zigzag wall made up of edge-sharing octahedra which propagate along the crystallographic $c$ axis (Fig. 1).

The four possible crystallographic positions of the $M$ ion are thus distinguished by their positions within these zigzag structures. In the $Fe_3BO_5$ system, the ions within the crystallographic sites 2 and 4 are involved in a structural transition at ≈280 K. Driven by a displacement of the central $Fe^2$ ion in alternate directions along the $Fe^4$-$Fe^2$-$Fe^4$ triad, this effectively doubles the lattice period along the crystallographic $c$ axis [3]. Interestingly, no such structural transition is reported either in the closely related $Co_3BO_5$ system or in any other heterometallic ludwigite.

Here, we report on the hitherto unexplored $Co_2AlBO_5$ system, and investigate it using temperature-dependent x-ray diffraction, specific heat, magnetization, and dielectric measurements. We observe the presence of a low-temperature reentrant *superspin*-glass-like state from within an (anti-ferro)magnetically ordered phase. Within this phase, a number of field-induced transitions are observed, which at the lowest measured temperatures manifest themselves in the form of sharp magnetization steps.

## II. EXPERIMENTAL TECHNIQUES

Small needlelike crystallites of $Co_2AlBO_5$ were synthesized using a reactive flux technique. Stoichiometric amounts of $Co_3O_4$ and $Al_2O_3$ were mixed with excess borax ($Na_2B_4O_7 \cdot 10H_2O$) in the ratio of 1:5, and ground well using a ball

*Corresponding author: sunil@iiserpune.ac.in

 

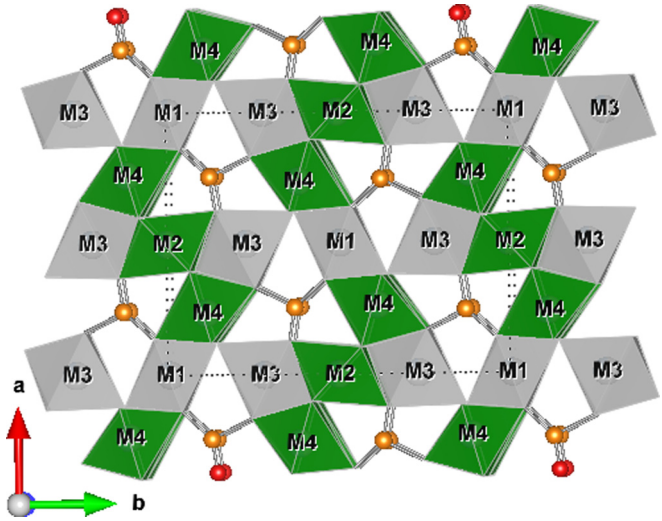


FIG. 1. The crystal structure of the homometallic ludwigite $M_3BO_5$ as viewed along the crystallographic $c$ axis. $M1$ to $M4$ depict the four distinct crystallographic positions which the transition metal can occupy within this structure.

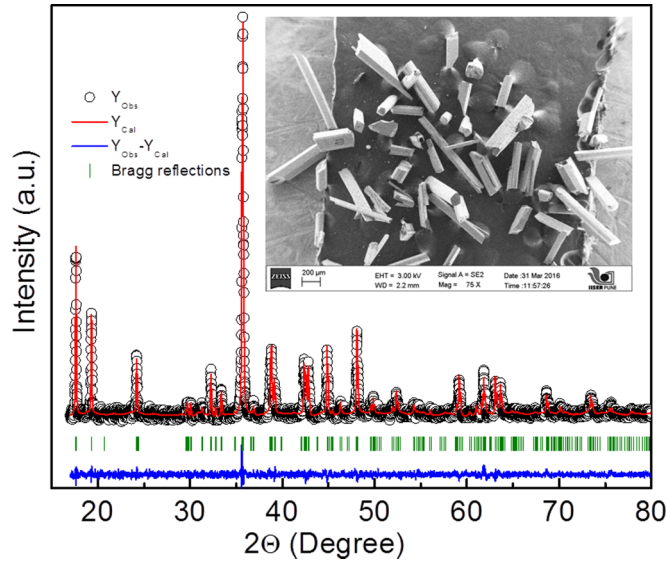


FIG. 2. A Rietveld fit to the room temperature x-ray diffraction data of $Co_2AlBO_5$. This corresponds to a fit with $R$ parameters of $R_{wp} = 14.0$, $R_e = 12.1$, and $\chi^2 = 1.34$. The inset shows a scanning electron micrograph where long needlelike crystallites are seen.

mill at 120 rpm for 12 hours to make a fine homogeneous mixture. This mixture was treated at 1000 °C for 90 hours in an alumina crucible followed by slow cooling to 740 °C (at the rate of 5 °C/hour), after which the furnace was turned off. Fine needlelike crystallites of the target material were extracted from the crucible and washed using warm dilute HCl and distilled water to remove the excess borax. Since these crystallites were too small for routine magnetic and thermodynamic measurements, they were crushed and treated as polycrystalline powders. Phase purity was confirmed using a Bruker D8 Advance diffractometer with Cu $K_\alpha$ radiation. Low-temperature x-ray diffraction was obtained using the powder diffractometer at beamline BL-18B, Photon Factory, KEK, Japan, using an x-ray wavelength of 0.8019 Å. Room temperature structural details were rigorously analyzed by the Rietveld method using the FULLPROF refinement program [14], and the variation in the lattice parameters of the low-temperature scans was determined using a Le Bail fit. Elemental compositions and their homogeneity were reconfirmed by using an energy dispersive x-ray spectrometer (Zeiss Ultra Plus). Specific heat and magnetization measurements were performed using a Quantum Design PPMS and an MPMS-XL SQUID magnetometer, respectively. Temperature-dependent dielectric measurements were performed in the standard parallel plate geometry, using an HP 4294A impedance analyzer. Measurements were done using an excitation ac signal of 1 V.

## III. RESULTS AND DISCUSSION

Room temperature x-ray diffraction of $Co_2AlBO_5$ revealed a single phase specimen, with no trace of any of the starting materials or any other impurity phases. A scanning electron micrograph reveals long needlelike crystallites as is shown in the inset of Fig. 2. A Rietveld refinement of the room temperature diffraction data is shown in the main panel of Fig. 2.

This system was seen to crystallize in an orthorhombic $Pbam$ symmetry [15], and the structural details of $Co_2AlBO_5$ as determined from the Rietveld refinement of room temperature x-ray diffraction data are summarized in Table I. All 4 crystallographic sites available for Co are seen to be diluted with the nonmagnetic Al, which is in contrast to that reported in the related $Co_{2.4}Ga_{0.6}BO_5$ system, where it was reported that Ga only occupies the $Co^2$ and $Co^4$ sites [10], with the $Co^4$

TABLE I. Structural parameters of $Co_2AlBO_5$ as determined from the Rietveld analysis of room temperature x-ray diffraction data.

$Co_2AlBO_5$
Temperature = 296 K
Space group: $Pbam$
Crystal system: Orthorhombic
$a = 9.2021(2)$ Å
$b = 12.0364(2)$ Å
$c = 2.9982(4)$ Å
$\alpha = \beta = \gamma = 90°$

| Atom | Wyckoff | $x/a$ | $y/b$ | $z/c$ | Fractional Occupation |
|---|---|---|---|---|---|
| $Co^1$ | 2b | 0 | 0 | −0.5 | 0.81 |
| $Al^1$ | 2b | 0 | 0 | −0.5 | 0.19 |
| $Co^2$ | 2c | 0.5 | 0 | 0 | 0.55 |
| $Al^2$ | 2c | 0.5 | 0 | 0 | 0.45 |
| $Co^3$ | 4h | 0.998(1) | 0.275(1) | −0.5 | 0.70 |
| $Al^3$ | 4h | 0.998(1) | 0.275(1) | −0.5 | 0.30 |
| $Co^4$ | 4g | 0.236(4) | 0.114(4) | 0 | 0.46 |
| $Al^4$ | 4g | 0.236(4) | 0.114(4) | 0 | 0.54 |
| $B^1$ | 4g | 0.257(2) | 0.376(2) | 0 | 1 |
| $O^1$ | 4g | 0.363(3) | 0.461(5) | 0 | 1 |
| $O^2$ | 4h | 0.121(1) | 0.134(1) | −0.5 | 1 |
| $O^3$ | 4g | 0.129(5) | 0.357(1) | 0 | 1 |
| $O^4$ | 4h | 0.398(1) | 0.073(1) | −0.5 | 1 |
| $O^5$ | 4g | 0.334(7) | 0.258(5) | 0 | 1 |

site being the most preferred one. In the case of $Co_2AlBO_5$, the $Co^4$ and $Co^1$ sites are found to be the most preferred and least preferred sites, respectively, for Al substitution. The chemical composition as obtained from the Rietveld analysis is $Co_{1.87}Al_{1.13}BO_5$.

The parent $Co_3BO_5$ system is reported to exhibit long-range antiferromagnetic order and diluting the magnetic lattice using nonmagnetic Al would be expected to reduce the temperature where long-range order sets in. Figure 3(a) shows the temperature dependence of the dc magnetization as measured in the $Co_2AlBO_5$ specimen. A bell-shaped feature, with a pronounced splitting between the zero-field-cooled (ZFC) and field-cooled (FC) measuring protocols, is observed. The temperature dependence of specific heat exhibits a small feature at around 42 K, which possibly corresponds to the onset of long-range magnetic ordering [Fig. 3(b)]. This also broadly coincides with the temperature at which the ZFC and FC curves bifurcate. Application of magnetic fields of the order of 8 T is seen to smear off this feature in the specific heat, as is seen in the inset. A Curie-Weiss fit to the inverse dc magnetic susceptibility in the high-temperature paramagnetic region as shown in the inset of Fig. 3(a) gives a Curie-Weiss temperature $\theta_{CW} = -9.19$ K. In comparison, the $\theta_{CW}$ values for $Fe_3BO_5$ and $Co_3BO_5$ are reported to be $-485$ K and $-25$ K, respectively [3,4]. It is evident that the variation of $\theta_{CW}$ in these ludwigites is not consistent with the temperatures at which long-range magnetic order is observed, since the ratio $|\theta_{CW}/T_N|$ is 6.9 and 0.6 for $Fe_3BO_5$ and $Co_3BO_5$, respectively. This anomalously small $|\theta_{CW}/T_N|$ value in the Co system was attributed to the predominance of ferromagnetic interactions, since ferromagnetically ordered rungs were thought to align antiparallel at the global $T_N$ [4]. This was also corroborated by larger values of the spontaneous magnetization determined from *M-H* isotherms within the magnetically ordered state. The $Co_2AlBO_5$ specimen investigated here exhibits a $|\theta_{CW}/T_N|$ value of 0.21, which is even smaller than that observed for the $Co_3BO_5$ system. This could be a consequence of the fact that nonmagnetic Al dilutes the magnetic sublattice. This could also indicate that Al substitution appears to favor the stabilization of ferromagnetic interactions at the cost of the antiferromagnetic ones. The effective magnetic moment per $Co^{2+}$ ion calculated from the Curie-Weiss fit is $3.5\mu_\beta$, which is close to the high spin value of $Co^{2+}$.

Crystallizing in similar orthorhombic ($Pbam$) structures at room temperatures, a striking difference between the Fe- and the Co-based ludwigites is the observation of a temperature-driven structural phase transition in the former, where a $Pbam \rightarrow Pbnm$ symmetry change occurs at ≈280 K [3]. On the contrary, the Co-based system has shown no evidence of such a transition at least down to ≈100 K [4], though it remains to be investigated whether such a transition exists at lower temperatures. Our temperature-dependent x-ray diffraction measurements on the $Co_2AlBO_5$ system down to 15 K clearly rule out the presence of a structural transition in this system, indicating that the absence of a structural transition appears to be a defining feature of all the Co-based ludwigites. However our measurements also indicate subtle changes in the lattice parameters as a function of temperature, and the effective change in the ratios $b/c$, $a/c$, and $b/a$ is shown in Fig. 3(c). Two distinct inflection points are seen, one at ≈150 K, which is not discernible in any other measurement, and the other at ≈50 K, which appears to coincide with the onset of long-range magnetic order. The latter indicates that the lattice and spin degrees of freedom could be strongly coupled in this system.

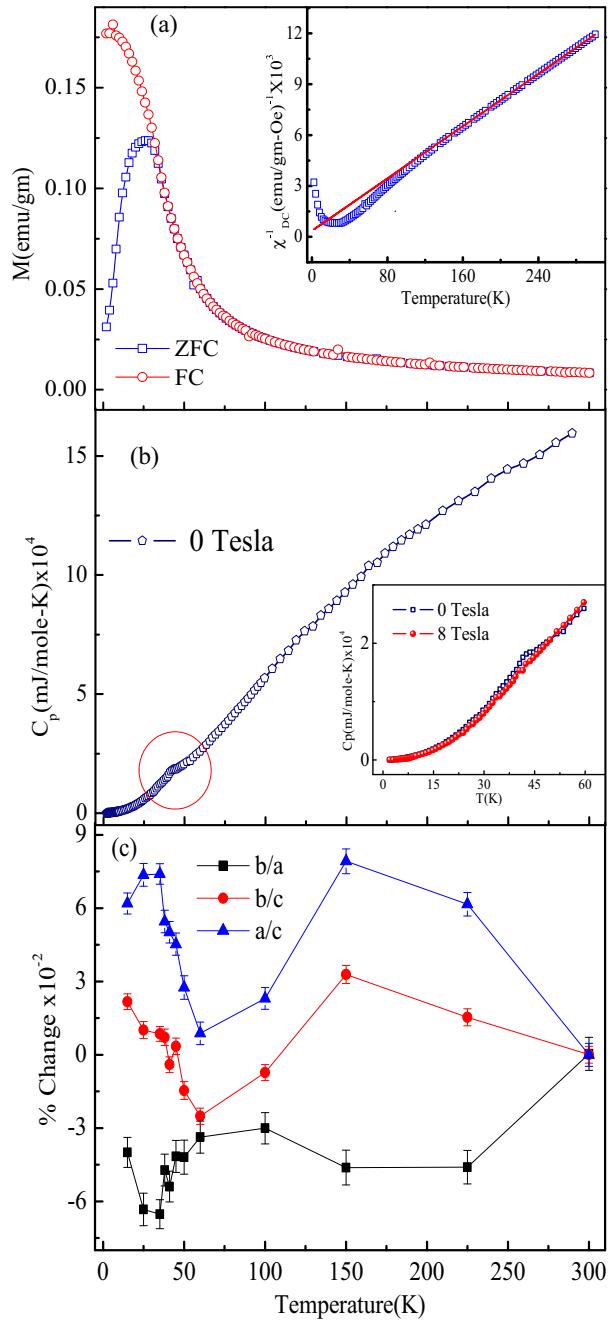


FIG. 3. Panel (a) depicts the temperature dependence of dc magnetization as measured in $Co_2AlBO_5$ in the zero-field-cooled (ZFC) and field-cooled (FC) protocols. The inset shows a Curie-Weiss fit in the high-temperature paramagnetic region. Panel (b) depicts the heat capacity as measured in the same sample in zero applied field, with a peak at ≈42 K indicating the onset of magnetic order. The inset shows the suppression of this feature with an applied magnetic field of 8 T. Panel (c) depicts the percent change in the lattice parameter ratios ($b/a$, $b/c$, and $a/c$ normalized with respect to their room temperature values), with a clear change being observed in the phase transition region.

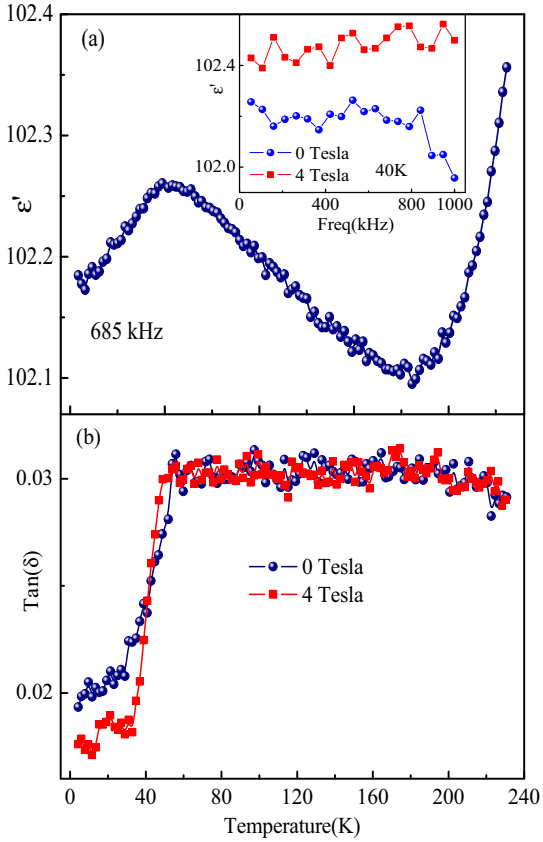


FIG. 4. Panel (a) depicts the temperature dependence of the real part of the dielectric constant $\epsilon'(T)$ (measured at a frequency of 685 kHz and an excitation voltage of 1 $V_{ac}$) which peaks at the magnetic ordering temperature. The inset shows a finite magnetoelectric effect as measured in isotherms of the dielectric constant $\epsilon'(H)$ at $T = 40$ K. Panel (b) shows the dielectric loss as measured at 0 and 4 T, with both of them exhibiting a sharp feature across the magnetic transition.

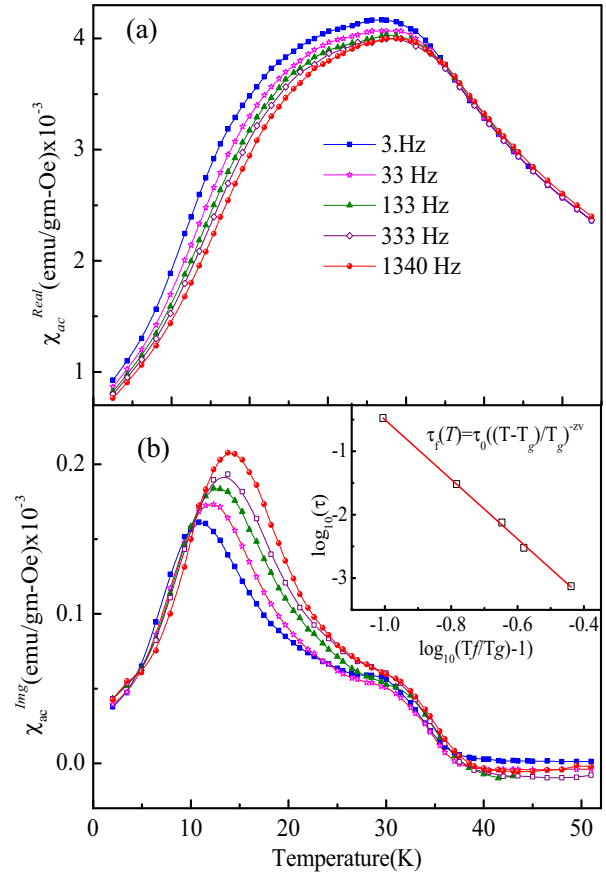


FIG. 5. The real (a) and the imaginary (b) parts of the ac magnetic susceptibility as measured in $Co_2AlBO_5$. The presence of a frequency-dependent low-temperature transition and a frequency-independent high-temperature one is clearly seen. The inset of (b) depicts dynamical scaling using $\tau/\tau_0 = [(T_f - T_G)/T_G)]^{z\nu}$, with the best fit giving $T_G = 10.6 \pm 0.2$ K and $z\nu = 4.7 \pm 0.5$.

Measurements of the dielectric constant in magnetic materials offer an interesting avenue of evaluating the coupling between the charge and magnetic degrees of freedom. To the best of our knowledge, there have been no reports of dielectric measurements of any member of the ludwigite family. Figure 4(a) depicts the real part of the dielectric constant as a function of temperature, as measured at 685 kHz.

A maximum in $\epsilon'(T)$ is observed in the vicinity of the magnetic transition, indicating a coupling of the electric and magnetic order parameters in this system. To further investigate this phenomenon, we have measured isotherms of the dielectric constant under zero and 4 T magnetic field within the magnetically ordered state, as is shown in the inset. A finite difference (≈0.6%) is observed, with $\epsilon'(H)$ being larger in the presence of an applied field. The magnetodielectric nature of $Co_2AlBO_5$ is also evident from the dielectric loss data [Fig. 4(b)], where a clear drop is observed in both the zero-field and in-field data near the magnetic-ordering temperature.

It is to be noted that there have been conflicting reports on the nature of the low-temperature magnetic ground state in the parent $Co_3BO_5$ system. Ivanova and co-workers [5] have reported a long-range magnetic transition with a $T_N \approx 45$ K, and a second magnetic transition at ≈17 K, as evidenced from a drop in the dc magnetization, coupled to a bifurcation of the ZFC and FC measurements. A subsequent publication [4] however reported only a solitary high-temperature transition at $T_N \approx 42$ K. Though ac susceptibility measurements within the magnetically ordered phase were highly frequency dependent, no clear signature of an additional low-temperature transition was observed in either the magnetic or thermodynamic measurements. It has also been suggested that the transition at ≈42 K is predominantly ferromagnetic, with an overriding weak antiferromagnetic component. In the absence of conclusive neutron diffraction data, the true magnetic structure of the $Co_3BO_5$ system remains undetermined. To investigate the possibility of an additional low-temperature transition in $Co_2AlBO_5$, we have performed frequency-dependent ac susceptibility measurements, as is shown in Fig. 5.

As seen in the upper panel, though a finite dispersion is observed at low temperatures in the real part of the ac magnetic susceptibility ($\chi^R_{ac}$), there is no clear evidence of an additional low-temperature transition. However, in the imaginary part of the susceptibility ($\chi^I_{ac}$), two clear transitions are observed, a frequency-independent high-temperature transition and a frequency-dependent low-temperature one.

The former is clearly associated with the onset of long-range (antiferro/ferri)magnetic order, with the latter characterizing the presence of a reentrant glassy phase.

The stabilization of a reentrant glassy phase from within a state with magnetic order is well known, and is known to exist in a number of different material classes including intermetallics [16], oxides [17], and interacting nanoparticle [18] systems. Unlike in a prototypical paramagnetic to spin glass transition, where disorder or mixed exchange interactions give rise to an *atomistic* glassy phase with frozen spins, these reentrant glasses are characterized by the freezing of *superspins* which could have ferromagnetic, antiferromagnetic, or ferrimagnetic order within. It has been unambiguously demonstrated that such systems exhibit a dynamic behavior analogous to that of prototypical spin glasses [19]. The inset of Fig. 5(b) shows a fit to a conventional critical slowing of the relaxation times given by $\tau/\tau_0 = [(T_f - T_G)/T_G)]^{z\nu}$. Here, $T_f(\omega)$ and $T_G$ refer to the freezing temperature characterized by the maximum in the $\chi'_{ac}$ and the true reentrant glass transition temperature, respectively. The best fit of the data, spanning from 3 Hz to 1.3 kHz, yields a glass transition temperature $T_G = 10.6 \pm 0.2$ K, a critical exponent $z\nu = 4.7 \pm 0.5$, and an effective spin-flip time $\tau_0$ of $10^{-6}$ seconds. We note that the value of $\tau_0$ in most atomistic spin glasses is of the order of $10^{-12}$ to $10^{-13}$ seconds [20–22], whereas in the case of interacting superparamagnets, values of the order of $10^{-6}$ to $10^{-9}$ seconds have been reported [23–25]. The fact that $\tau_0 \approx 10^{-6}$ seconds in our case is clearly a consequence of the fact that the magnetic entity under consideration here is made up of a large number of spins. We also note that the critical exponent $z\nu$ in our case appears to be smaller than that observed in most spin glass transitions.

The glassy nature of the low-temperature magnetic ground state is also reflected in the analysis of the specific heat measurements. Figure 6 shows the linear fit to the low-temperature specific heat using the equation $C/T = \gamma + \beta T^2$,

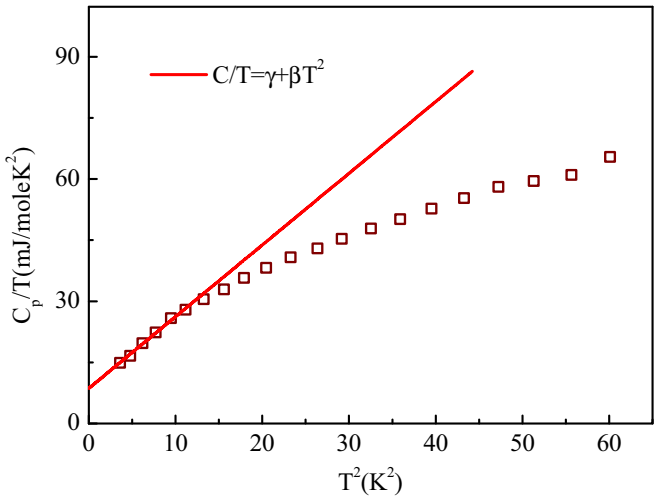


FIG. 6. The specific heat of $Co_2AlBO_5$ plotted as $C/T$ versus $T^2$, with the linear fit for $T < 4$ K indicating that the data can be described by the equation $C/T = \gamma + \beta T^2$. The values of $\gamma$ and $\beta$ obtained from this fit are $8.6 \pm 0.6$ mJ/mol K$^2$ and $1.75 \pm 0.07$ mJ/mol K$^2$, respectively.

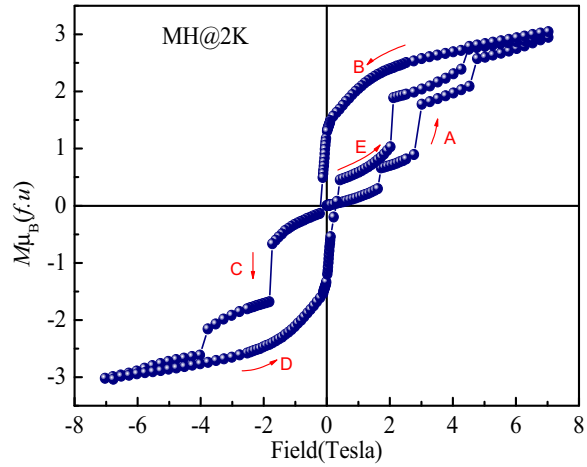


FIG. 7. The magnetization isotherm of $Co_2AlBO_5$ as measured at 2 K, exhibiting a number of sharp magnetization steps.

giving values of $8.6 \pm 0.6$ mJ/mol K$^2$ and $1.75 \pm 0.07$ mJ/mol K$^2$ for $\gamma$ and $\beta$, respectively. The large value of $\gamma$ in the ludwigites has earlier been attributed to magnetic frustration in these materials [26]. It is to be noted that the value of $\gamma$ in the case of $Co_2AlBO_5$ is more than twice as large as that reported for the undiluted homometallic Co-based ludwigite.

The only other ludwigite with a larger $\gamma$ is the system $Co_5Ti(O_2BO_3)_2$ which was reported to stabilize in a low-temperature spin glass phase, exhibiting a conventional paramagnetic to spin glass transition at $T_G \approx 19$ K [27]. The value of the Debye temperature ($\theta_D$) using the relation ${\theta_D}^3 = 243R/\beta$ (with $R$ being the universal gas constant) gives a value of 104.7 K, which is smaller than that determined earlier for the undiluted $Co_3BO_5$ system.

The $Co_3BO_5$ system is reported to exhibit a uniaxial anisotropy, with the easy direction of magnetization lying along the crystallographic $b$ axis [8]. Below $T \leqslant 20$ K, a stiffening of the hardness has also been suggested from measurements of the magnetic coercivity $H_C(T)$. An $M$-$H$ isotherm as measured at 2 K for the $Co_2AlBO_5$ system is shown in Fig. 7, with the direction of the field cycles being denoted by $A \rightarrow E$.

The fact that saturation is not reached till the highest applied magnetic fields indicates that at least some part of the sample persists in an antiferromagnetic phase right up to 7 T. However, a striking observation is that the magnetization of $Co_2AlBO_5$ is seen to exhibit sharp steps, exhibiting a staircase-like behavior. Such sharp magnetization steps are now known to occur in a few strongly correlated systems, and are thought to arise from a number of distinct physical processes. For instance, in the spin chain compound $Ca_3Co_2O_6$, well-separated magnetization steps (and plateaus) are thought to arise from the quantum tunneling of magnetization [28]. First postulated in the context of molecular magnets such as $Mn_{12}$ acetate [29] and the $Fe_8$ molecular nanomagnets [30], this relies on the magnetic field facilitating resonant tunneling in systems characterized by a large spin values and an Ising-like anisotropy. Sharp magnetization steps have also been observed in site-diluted antiferromagnets of the form $Fe_xMg_{1-x}Cl_2$ [31] and disordered systems such as $CeNi_{1-x}Cu_x$ [32], where they have been

attributed to a field-induced avalanche of flipping domains. Explained within the framework of the random field Ising model, these magnetization steps are typically characterized by the fact that their position appears to change in different measurement runs—no evidence of which is seen in our data.

More recently, sharp magnetization steps have been reported in a number of transition metal oxides, where a martensitic scenario has been invoked. Gaining prominence in the context of phase-separated manganites [33–36], this scenario has also been used to explain magnetization steps in other material classes, including a recent report in an itinerant electron system $LaFe_{12}B_6$ [37]. The mechanism here pertains to the catastrophic evolution of the antiferromagnetic (AFM)–ferromagnetic (FM) phase boundary when the applied magnetic field is used to change the predominantly AFM ground state to a FM one. The steps in magnetization are thus observed when the magnetization energy is minimized at the cost of the elastic energy at the AFM-FM interfaces. This was reminiscent of the growth of the martensite phase across an austenite-martensite phase transition, where the elastic strain at the interface between these two phases is relieved in sharp discontinuous steps. The glassy low-temperature ground state of $Co_2AlBO_5$ where both ferromagnetic and antiferromagnetic interactions are thought to coexist could well belong to this class.

We note that magnetization steps have been reported earlier in polycrystalline specimens of a related ludwigite $Co_5Ti(O_2BO_3)_2$, which also exhibits a glassy low-temperature ground state [27]. However, in that case the abrupt increase in the magnetization was conjectured to arise from a field-driven rotation of the effective magnetization from the hard to the easy axis. The glasslike ground state of $Co_5Ti(O_2BO_3)_2$ also appears to be different from the one we observe in $Co_2AlBO_5$. In the former, a spin glass state is seen to arise directly from the high-temperature paramagnetic state as a consequence of competing ferromagnetic and antiferromagnetic interactions. In the latter, the glassy state is a reentrant one, which arises from within an antiferromagnetically ordered state, and is associated with the freezing of magnetic clusters. This is clearly borne out from the nature of frequency-dependent ac susceptibility data, as well the large value of the spin-flip time $\tau_0$.

We have also evaluated the evolution of the critical fields at which these magnetization steps occur, as a function of the temperature, as shown in Fig. 8. Here, all the isotherms depict the first magnetization curve alone, and the system was heated to room temperatures between two consecutive isotherms. Traces of the three magnetization steps, which we observe in the *M-H* isotherm at 2 K, are also discernible in the form of a change of slope in the *M-H* isotherms measured at higher temperatures. Using curves of $dM/dH$, we observe that these critical fields can be identified all throughout the magnetic phase, and they are depicted in the lower panel of Fig. 8. It is evident that the critical fields associated with the metamagnetic transitions remain invariant with the measured temperatures right down to about 10 K, below which a monotonic increase of the critical field is observed. The fact that the magnetization has not saturated implies that additional metamagnetic transition(s) would possibly be observed at higher magnetic fields, before the system completely transforms to a ferromagnetic state.

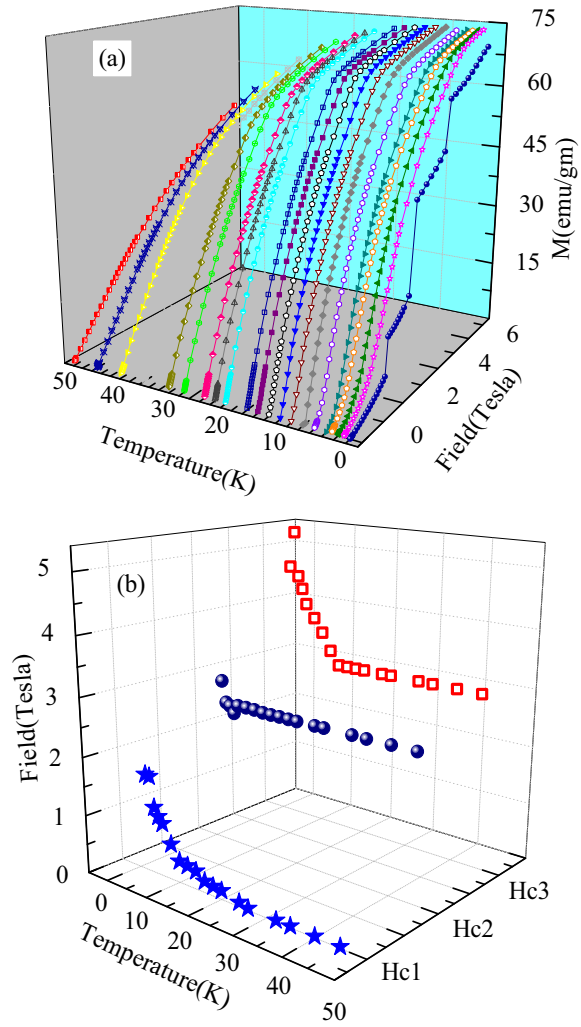


FIG. 8. Panel (a) depicts isotherms of the first magnetization curve of $Co_2AlBO_5$ measured from 2 K to 40 K. The presence of 3 metamagnetic transitions can be deduced from $dM/dH$, and the critical fields associated with these transitions ($H_{C1}$, $H_{C2}$, and $H_{C3}$) are plotted in (b) as a function of temperature ($T$) and applied magnetic field ($H$).

## IV. CONCLUSIONS

In summary, we have investigated the structural, thermodynamic, magnetic, and dielectric properties of the oxyborate $Co_2AlBO_5$. This system is seen to crystallize in an orthorhombic *Pbam* symmetry, and exhibits no evidence of a structural transition down to the lowest measured temperatures. This is in sharp contrast to the Fe-based ludwigite $Fe_3BO_5$, which is characterized by a doubling of the unit cell along the crystallographic $c$ axis at $T \approx 280$ K, and highlights the difference between the Co- and Fe-based systems. On cooling, $Co_2AlBO_5$ exhibits an antiferro/ferrimagnetic transition at 42 K, followed by a superspin glass transition at $T_G = 10.6$ K. Interestingly, a number of metamagnetic transitions are observed, which at the lowest temperatures they manifest themselves in the form of sharp magnetization steps, reminiscent of those observed in the mixed valent manganites.

## ACKNOWLEDGMENTS

The authors thank D. Buddhikot, A. M. Patade, and A. Prathamshetti for their help in heat capacity, dielectric, and energy dispersive x-ray measurements respectively. J.K. acknowledges DST India for a SERB-NPDF. S.N. acknowledges the Department of Science and Technology (DST, Government of India) for support through Grant No. SB/S2/CMP-048/2013, and for funding support under the DST Nanomission Thematic Unit Program. J.K. and S.N. also thank the Department of Science and Technology, India for the financial support and Saha Institute of Nuclear Physics, India for facilitating the experiments at the Indian Beamline, Photon Factory, KEK, Japan.



[1] R. B. Guimarães, M. Mir, J. C. Fernandes, M. A. Continentino, H. A. Borges, G. Cernicchiaro, M. B. Fontes, D. R. S. Candela, and E. Baggio-Saitovitch, Phys. Rev. B **60**, 6617 (1999).

[2] J. C. Fernandes, R. B. Guimarães, M. A. Continentino, L. Ghivelder, and R. S. Freitas, Phys. Rev. B **61**, R850 (2000).

[3] M. Mir, R. B. Guimarães, J. C. Fernandes, M. A. Continentino, A. C. Doriguetto, Y. P. Mascarenhas, J. Ellena, E. E. Castellano, R. S. Freitas, and L. Ghivelder, Phys. Rev. Lett. **87**, 147201 (2001).

[4] D. C. Freitas, M. A. Continentino, R. B. Guimarães, J. C. Fernandes, J. Ellena, and L. Ghivelder, Phys. Rev. B **77**, 184422 (2008).

[5] N. B. Ivanova, A. D. Vasil'ev, D. A. Velikanov, N. V. Kazak, S. G. Ovchinnikov, G. A. Petrakovskiĭ, and V. V. Rudenko, Phys. Solid State **49**, 651 (2007).

[6] N. V. Kazak, N. B. Ivanova, V. V. Rudenko, A. D. Vasil'ev, D. A. Velikanov, and S. G. Ovchinnikov, Phys. Solid State **51**, 966 (2009).

[7] L. Bezmaternykh, E. Kolesnikova, E. Eremin, S. Sofronova, N. Volkov, and M. Molokeev, J. Magn. Magn. Mater. **364**, 55 (2014).

[8] J. Bartolomé, A. Arauzo, N. V. Kazak, N. B. Ivanova, S. G. Ovchinnikov, Y. V. Knyazev, and I. S. Lyubutin, Phys. Rev. B **83**, 144426 (2011).

[9] Y. V. Knyazev, N. B. Ivanova, O. A. Bayukov, N. V. Kazak, L. N. Bezmaternykh, and A. D. Vasiliev, Phys. Solid State **55**, 1175 (2013).

[10] N. B. Ivanova, M. S. Platunov, Y. V. Knyazev, N. V. Kazak, L. N. Bezmaternykh, A. D. Vasiliev, S. G. Ovchinnikov, and V. I. Nizhankovskii, Phys. Solid State **54**, 2212 (2012).

[11] H. Neuendorf and W. Guner, J. Magn. Magn. Mater. **173**, 117 (1997).

[12] G. A. Petrakovskiĭ, L. N. Bezmaternykh, D. A. Velikanov, M. S. Malokeev, O. A. Bayukov, A. M. Vorotynov, and R. Szymchak, Phys. Solid State **51**, 2486 (2009).

[13] N. B. Ivanova, M. S. Platunov, Y. V. Knyazev, N. V. Kazak, L. N. Bezmaternykh, E. V. Eremin, and A. D. Vasiliev, Low Temp. Phys. **38**, 172 (2012).

[14] J. Rodriguez-Carvajal, *An Introduction to the Programme FULLPROF* (Laboratoire Leon Brillouin, CEA-CNRS, Saclay, France, 2001).

[15] J. Hriljac, R. Brown, A. Cheetham, and L. Satek, J. Solid State Chem. **84**, 289 (1990).

[16] K. Jonason, J. Mattsson, and P. Nordblad, Phys. Rev. B **53**, 6507 (1996).

[17] P. A. Kumar, R. Mathieu, P. Nordblad, S. Ray, O. Karis, G. Andersson, and D. D. Sarma, Phys. Rev. X **4**, 011037 (2014).

[18] K. Hiroi, K. Komatsu, and T. Sato, Phys. Rev. B **83**, 224423 (2011).

[19] R. Mathieu, J. A. D. Toro, D. Salazar, S. S. Lee, J. L. Cheong, and P. Nordblad, Europhys. Lett. **102**, 67002 (2013).

[20] C. Dekker, A. F. M. Arts, H. W. de Wijn, A. J. van Duyneveldt, and J. A. Mydosh, Phys. Rev. B **40**, 11243 (1989).

[21] R. Mathieu, A. Asamitsu, Y. Kaneko, J. P. He, and Y. Tokura, Phys. Rev. B **72**, 014436 (2005).

[22] S. Nair and A. K. Nigam, Phys. Rev. B **75**, 214415 (2007).

[23] E. Wandersman, V. Dupuis, E. Dubois, R. Perzynski, S. Nakamae, and E. Vincent, Europhys. Lett. **84**, 37011 (2008).

[24] X. Chen, S. Bedanta, O. Petracic, W. Kleemann, S. Sahoo, S. Cardoso, and P. P. Freitas, Phys. Rev. B **72**, 214436 (2005).

[25] S. Sahoo, O. Petracic, C. Binek, W. Kleemann, J. B. Sousa, S. Cardoso, and P. P. Freitas, Phys. Rev. B **65**, 134406 (2002).

[26] D. C. Freitas, M. A. Continentino, R. B. Guimarães, J. C. Fernandes, E. P. Oliveira, R. E. Santelli, J. Ellena, G. G. Eslava, and L. Ghivelder, Phys. Rev. B **79**, 134437 (2009).

[27] D. C. Freitas, R. B. Guimarães, D. R. Sanchez, J. C. Fernandes, M. A. Continentino, J. Ellena, A. Kitada, H. Kageyama, A. Matsuo, K. Kindo, G. G. Eslava, and L. Ghivelder, Phys. Rev. B **81**, 024432 (2010).

[28] A. Maignan, V. Hardy, S. Hebert, M. Drillon, M. R. Lees, O. Petrenko, D. M. K. Paul, and D. Khomskii, J. Mater. Chem. **14**, 1231 (2004).

[29] J. R. Friedman, M. P. Sarachik, J. Tejada, and R. Ziolo, Phys. Rev. Lett. **76**, 3830 (1996).

[30] C. Sangregorio, T. Ohm, C. Paulsen, R. Sessoli, and D. Gatteschi, Phys. Rev. Lett. **78**, 4645 (1997).

[31] J. Kushauer, R. van Bentum, W. Kleemann, and D. Bertrand, Phys. Rev. B **53**, 11647 (1996).

[32] N. Marcano, J. C. Gómez Sal, J. I. Espeso, L. Fernández Barquín, and C. Paulsen, Phys. Rev. B **76**, 224419 (2007).

[33] R. Mahendiran, A. Maignan, S. Hébert, C. Martin, M. Hervieu, B. Raveau, J. F. Mitchell, and P. Schiffer, Phys. Rev. Lett. **89**, 286602 (2002).

[34] V. Hardy, A. Maignan, S. Hébert, C. Yaicle, C. Martin, M. Hervieu, M. R. Lees, G. Rowlands, D. M. K. Paul, and B. Raveau, Phys. Rev. B **68**, 220402 (2003).

[35] F. M. Woodward, J. W. Lynn, M. B. Stone, R. Mahendiran, P. Schiffer, J. F. Mitchell, D. N. Argyriou, and L. C. Chapon, Phys. Rev. B **70**, 174433 (2004).

[36] S. Nair, A. K. Nigam, A. V. Narlikar, D. Prabhakaran, and A. Boothroyd, Phys. Rev. B **74**, 132407 (2006).

[37] L. V. B. Diop, O. Isnard, and J. Rodríguez-Carvajal, Phys. Rev. B **93**, 014440 (2016).